


# Restorative effects of human neural stem cell grafts on the primate spinal cord

Ephron S Rosenzweig<sup>1</sup>, John H Brock<sup>1,2</sup>, Paul Lu<sup>1,2</sup>, Hiromi Kumamaru<sup>1</sup>, Ernesto A Salegio<sup>3</sup>, Ken Kadoya<sup>1,4</sup>, Janet L Weber<sup>1</sup>, Justine J Liang<sup>1</sup>, Rod Moseanko<sup>3</sup>, Stephanie Hawbecker<sup>3</sup>, J Russell Huie<sup>5</sup>, Leif A Havton<sup>6</sup>, Yvette S Nout-Lomas<sup>7</sup> , Adam R Ferguson<sup>5,8</sup> , Michael S Beattie<sup>5</sup>, Jacqueline C Bresnahan<sup>5</sup> & Mark H Tuszynski<sup>1,2</sup>

**We grafted human spinal cord–derived neural progenitor cells (NPCs) into sites of cervical spinal cord injury in rhesus monkeys (*Macaca mulatta*). Under three-drug immunosuppression, grafts survived at least 9 months postinjury and expressed both neuronal and glial markers. Monkey axons regenerated into grafts and formed synapses. Hundreds of thousands of human axons extended out from grafts through monkey white matter and synapsed in distal gray matter. Grafts gradually matured over 9 months and improved forelimb function beginning several months after grafting. These findings in a ‘preclinical trial’ support translation of NPC graft therapy to humans with the objective of reconstituting both a neuronal and glial milieu in the site of spinal cord injury.**

Three decades of spinal cord injury (SCI) research have made it clear that abundant, long-distance regeneration of injured axons, which might improve function below a lesion site, remains elusive<sup>1</sup>. Numerous extrinsic mechanisms, including an inhibitory extracellular matrix that develops around the site of injury<sup>2,3</sup>, inhibitory myelin-associated proteins<sup>4,5</sup>, and a lack of growth-promoting factors, such as neurotrophins<sup>6</sup>, in appropriate spatial and temporal gradients for promotion of growth, contribute to failure of axonal regeneration after SCI.

Failure of neuron-intrinsic mechanisms also contributes to the lack of axonal regeneration in adult central nervous system (CNS), and enhancing those intrinsic neuronal growth mechanisms overcomes extrinsic inhibitors<sup>7,8</sup>. For example, neurons derived from developing spinal cord have active growth programs that support robust axon extension and may be insensitive to inhibitors present in adult CNS<sup>9–11</sup>. This suggests recovery after SCI may be improved through an alternative approach: grafting neural progenitor and neural stem cells into the injury site to form a neuronal relay circuit across the gap<sup>9–15</sup>. Such relay circuits are conceptually similar to those formed by propriospinal circuits after incomplete SCI<sup>16</sup>. To create such a circuit, a critical mass of grafted cells must: (i) survive and differentiate into neurons; (ii) support growth of injured host axons into the graft; (iii) accept synapses from these host-derived axons; (iv) extend axons into the host spinal cord; and (v) form synapses on host neurons below the lesion (**Fig. 1a**). Building on this concept, we recently optimized methods for grafting neural stem cells to sites of SCI in rodents that improve electrophysiological and functional outcomes after even severe SCI<sup>17–19</sup>. Moreover, spinal cord retranssection immediately rostral to an established graft reverses electrophysiological and

functional recovery, supporting the hypothesis that these implants form new neural relays across the lesion<sup>17</sup>. These findings support the possibility that neural stem cell grafting could promote neural repair after human SCI.

A nonhuman primate model of SCI can address numerous points related to clinical translation, including species differences in (i) intrinsic stem cell biology, procurement, and maturation; (ii) CNS size and functional neuroanatomy; and (iii) immune mechanisms<sup>20–23</sup>. Indeed, a number of experimental therapies showing efficacy in rodent models may be ineffective or impractical in primates<sup>24</sup>; these therapies may fail for numerous reasons, including differences in intrinsic biology, small effect sizes, poor safety and tolerability, and lack of scalability to humans of methods developed in rodents<sup>25</sup>. Primate studies can be of great importance in addressing these issues before human clinical trials<sup>24</sup>. Indeed, recent reports support the paramount importance of the validation of translational programs before human implementation<sup>26</sup>, and proof of principle in a primate model is key in this endeavor<sup>24</sup>.

We now report successful engraftment of human spinal cord–derived multipotent neural progenitor cells into rhesus monkeys after SCI. Human neural progenitor cells extend up to hundreds of thousands of axons through degenerating white matter into the host spinal cord and form reciprocal synaptic connections with host circuits. Grafts are safe and well-tolerated and improve functional outcomes.

## RESULTS

A total of nine adult male rhesus monkeys underwent implantation of human spinal cord–derived neural progenitor cells. Monkeys received right-side C7 hemisection lesions as previously described<sup>27</sup>

<sup>1</sup>Department of Neurosciences, University of California, San Diego, La Jolla, California, USA. <sup>2</sup>Veterans Administration Medical Center, La Jolla, California, USA.

<sup>3</sup>California National Primate Research Center, University of California, Davis, Davis, California, USA. <sup>4</sup>Department of Orthopaedic Surgery, Hokkaido University, Sapporo, Japan. <sup>5</sup>Department of Neurosurgery, University of California, San Francisco, San Francisco, California, USA. <sup>6</sup>Department of Neurology, University of California, Los Angeles, Los Angeles, California, USA. <sup>7</sup>College of Veterinary Medicine and Biomedical Sciences, Colorado State University, Fort Collins, Colorado, USA. <sup>8</sup>Veterans Administration Medical Center, San Francisco, California, USA. Correspondence should be addressed to M.H.T. ([mtuszynski@ucsd.edu](mailto:mtuszynski@ucsd.edu)).

Received 3 March 2017; accepted 26 January 2018; published online 26 February 2018; doi:10.1038/nm.4502

2 weeks before grafting. This 2-week delay after injury is a clinically relevant time period in which humans might be expected to medically stabilize before undergoing neural stem cell therapy. On the day of grafting, the spinal cord lesion site was surgically re-exposed, and scar tissue on the dorsal aspect of the spinal cord was incised (Fig. 1b,c). Viscous fluid containing cellular debris was released from the lesion site, and the open lesion cavity was microscopically visualized in its entirety and freed of internal adhesions if present. A total of 20 million cells were then grafted into the lesion cavity using sterilized 100- $\mu$ l pipettors held freehand. Grafted cells were GFP-expressing human multipotent neural progenitor cells isolated from an 8-week-old human embryonic spinal cord and maintained as a stable cell line (566RSC-UBQT line)<sup>28–30</sup>. Cells were shipped overnight from Maryland to the University of California, Davis primate research center and arrived on the day of implantation. Immediately before grafting, cells were suspended in a growth factor cocktail and fibrin–thrombin matrix as employed in rodent experiments<sup>17,18</sup> (Online Methods).

### Development of grafting methods

Highlighting the vital importance of large animal models in translational studies, our initial efforts to transplant human neural progenitor cells into four monkeys failed to support graft survival despite use of methods that were successful in rodents. First, we found that cerebrospinal fluid (CSF) rapidly filled the lesion cavity and washed away grafted cells despite the use of a rapidly gelling fibrin–thrombin matrix. Thus, the first two subjects had no surviving cells. Employing a historical method for draining CSF in humans, we tilted the operative table to a 30° angle immediately before grafting to drain CSF from the cervical spinal cord in all subsequent monkeys; this action provided a 15-min period in which the lesion cavity was free of CSF. We also increased the fibrin–thrombin concentration in the grafting mixture to generate rapid gelling (within 3 s). These measures resulted in filling of the lesion site with cells at the conclusion of the grafting session in the next two subjects. However, when examined 2 months later, cells failed to fill the entire lesion cavity, although some graft cell survival was evident. Monkeys up to this point had been immunosuppressed with low initial doses of mycophenolate mofetil and tacrolimus (Online Methods). Beginning with Subject 5, we adopted a more robust immunosuppressive regimen to prevent rejection of the clinically transplanted organ. It comprised higher initial doses of mycophenolate mofetil and tacrolimus and more frequent monitoring (two or three times per week) of immunosuppressant drug levels until therapeutic doses were well established. Using these optimized methods, graft survival and fill of the lesion site were achieved in the five subsequent subjects (Fig. 1d and Supplementary Fig. 1).

### Human stem cell grafts survive and extend large numbers of axons over long distances in the lesioned primate spinal cord

NPCs in the five subsequent subjects survived in C7 hemisection lesion cavities from 2 through 9 months after grafting (Fig. 1d and Supplementary Fig. 1). Grafts occupied the majority of the lesion cavity in all subjects and integrated well with the host spinal cord. Neuronal markers were readily detectable in grafts at all monitored time points (2–9 months after grafting; Fig. 1). The early neuronal marker doublecortin was predominant at 2 months postgrafting and declined but remained detectable after 9 months (Fig. 1g). The more mature neuronal marker NeuN was also detected at 2 months postgrafting (Fig. 1e,f) and continued to be expressed over time. The density of cells in the graft was highest at 2 months postimplantation (400,000 cells per mm<sup>3</sup> graft) and steadily dropped 63% to 150,000 cells per mm<sup>3</sup>

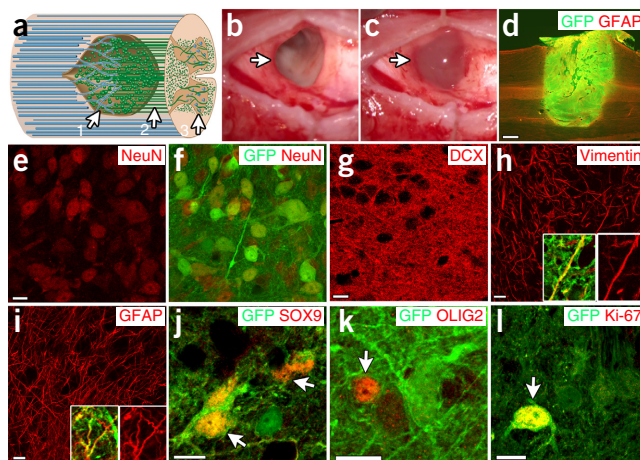


**Figure 1** Graft concept, procedure, survival, and differentiation. (a) Schematic of neural stem cell grafting and functional relay formation across a contusion injury site (brown). Host axons (blue) grow into the graft (1), graft axons (green) grow into the host spinal cord (2) to complete the relay circuit (3). (b) Surface of monkey spinal cord with dura retracted laterally and lesion cavity visible (arrow). (c) After grafting, the slightly opaque suspension of human NPCs in the fibrin matrix is visible in the lesion site (arrow). (d) Horizontal section of rhesus monkey C7 hemisection lesion site showing the human spinal cord neural progenitor cell graft (GFP+) is well-integrated into the injury site. Section is rostral to the left. (e, f) Images of NeuN labelling only (e) and merged NeuN and GFP labelling (f) in a 5-month-old graft. (g, h) Labelling for doublecortin (DCX; early neuronal marker; g) and vimentin (early glial marker; h), which were present in all grafts. (i) Labelling for GFAP (mature astrocyte marker) was only present in 5- and 9-month-old grafts (5-month-old graft shown). Insets of vimentin and GFAP labelling are shown in h and i, respectively, with and without GFP. (j) Labelling for SOX9 (astrocyte and ependymal cell marker), which was present in all grafts (arrows); at 5 and 9 months, 80% of these cells were astrocytes (GFAP+). (k) Labelling for OLIG2, which was present in all grafts (arrow). (l) Labelling for Ki-67 (a dividing cell marker), which was observed at low (1.5%) but detectable levels (arrow) at all time points. Scale bars: d, 1 mm; e–l, 10  $\mu$ m. e and f consist of five 0.5- $\mu$ m confocal optical planes; g, j, k, and l consist of two 0.5- $\mu$ m confocal optical planes; h and i are single 0.5- $\mu$ m confocal optical planes.

at 9 months postgrafting ( $R^2 = 0.93$ ,  $P = 0.007$ ; Fig. 2a and Table 1). In contrast, cell size steadily increased over the same time period ( $R^2 = 0.82$ ,  $P = 0.03$ ; Fig. 2b and Table 1). Grafts expressed vimentin, a filamentous marker of early astrocytes, at 2 months postimplantation, the earliest time point examined (Fig. 1h). Glial fibrillary acidic protein (GFAP), a marker of more mature astrocytes, did not detectably colocalize with GFP until 5 months postgrafting (Fig. 1i), suggesting a prolonged period of astrocyte maturation as well. The relative proportions of cells expressing a marker for one of the three cardinal cell types of the CNS, namely neuronal cells (NeuN), astrocytes (SOX9), and oligodendrocytes (OLIG2), were  $57 \pm 10\%$ ,  $26 \pm 5\%$ , and  $17 \pm 7\%$  (mean  $\pm$  s.e.m.), respectively (Fig. 1e, j, k); these proportions were calculated from an analysis of  $766 \pm 100$  (mean  $\pm$  s.e.m.) individual cells per subject. Astrocyte identity was confirmed in 80% of SOX9<sup>+</sup> cells through GFAP colabeling in Subjects 8 and 9 (refs. 31,32). Oligodendrocyte lineage was confirmed in all OLIG2<sup>+</sup> cells through a lack of colabeling with insulin gene enhancer proteins 1 and 2 (ISL1 and ISL2; data not shown); the lack of graft-derived cell migration (see below) suggests that these cells are likely immature nonmyelinating oligodendrocytes. No graft-derived cells expressed Opalin, a marker of mature myelinating oligodendrocytes<sup>33</sup> (Supplementary Fig. 2),

indicating that mature oligodendrocytes were not yet present in grafts. The proportion of dividing cells in grafts, as assessed through Ki-67 labeling (Fig. 11), was low at all examined time points ( $1.5 \pm 0.5\%$ , mean  $\pm$  s.e.m.); it was 0.7% at 9 months postgrafting. Teratomas or tumors were not detected in any subject.

Notably, human axons emerged from grafts in extraordinary numbers and over long distances. Up to 150,000 graft-derived axons were present 2 mm caudal to the lesion 2–9 months postgrafting (Figs. 2 and 3, Table 1, and Supplementary Fig. 1), and axons reached distances of up to 50 mm from the graft (Supplementary Fig. 3). Axons emerged rostrally in similar numbers and over similar distances (Supplementary Fig. 3). Axons extended into white matter tracts that were directly abutted against grafts and appeared to maintain growth within these same white matter fascicles reaching points distant from the graft (Supplementary Fig. 4); this observation suggests that axons may continue to extend through the white matter tracts that they first encounter upon emerging from grafts in the lesion site. Furthermore, the fact that human axons extended linearly through host white matter (Fig. 3 and Supplementary Figs. 1, 3, and 4) suggests that adult myelin does not inhibit the growth of these human axons at this developmental stage, which is a finding consistent with observations in nonprimate models<sup>9–12,17–19</sup>.

Emerging axons expressed class III  $\beta$ -tubulin, a marker of both immature and mature axons; light-chain neurofilament (NF70), a marker of both immature and mature small-diameter axons; and unphosphorylated heavy-chain neurofilament (SMI32), another immature axon marker (Supplementary Fig. 5). Graft-derived axons did not express phosphorylated heavy-chain neurofilament (NF200; Fig. 4f, inset), a marker expressed in many mature human axons (Supplementary Fig. 6). Thus, axons were not fully mature even 9 months postgrafting; this is consistent with neuronal size measures and delayed expression of GFAP as noted above and with delayed maturation of other human neural stem cells in rat SCI<sup>34</sup>. Synapse formation was readily detected between graft-derived axons and host neurons in the spinal cord caudal to the lesion site as reflected both by apposition of postsynaptic HOMER1 with presynaptic GFP and synaptophysin and by results from ultrastructural analysis (Fig. 3 and Supplementary Figs. 7 and 8). Extending human axons frequently converged onto host motor neurons, wrapping motor neuronal somata with dozens of appositions that colocalized with the synaptic marker synaptophysin (Fig. 3f,g). Ultrastructurally, all observed graft–host synapses had clear, spheroid vesicles in the presynaptic bouton, and synaptic specializations in the plane of sectioning were characteristically asymmetric, features indicative of an excitatory phenotype (Fig. 3h–j and Supplementary Fig. 8), as expected of long-projecting axons<sup>35</sup>. Consistent with the apparent immature

state of graft-derived axons, myelination of graft-derived axons that were caudal to the lesion site and up to 1  $\mu$ m diameter was not detected in the 9 months following grafting (Supplementary Fig. 6). In contrast, axons emerging from more rapidly maturing rat neural progenitor cells grafted into rats are readily myelinated by 2 months postimplantation<sup>17</sup>.

### Host axons regenerate into human neural stem cell grafts

In theory, human neural stem cell implantation into a lesion cavity aims to re-establish a neuronal relay across a site of SCI. For this to occur, host axons must regenerate into neural stem cell grafts, and neural stem cells must extend axons out of these grafts and into the host spinal cord. To assess whether host axons regenerate into human neural progenitor cell grafts, we performed immunolabeling for NF200 (which is not expressed by grafted neurons; Fig. 4f, inset) and serotonergic motor axons, and we performed anterograde tracing of the corticospinal system using intracortical injections of biotinylated dextran amine (BDA). Notably, grafts were extensively and densely penetrated by host NF-200-labeled axons beginning 2 months postgrafting and persisting through 9 months (Fig. 4e,f). Many NF200-labeled axons originated from intraspinal neuronal circuits. Serotonergic axons, critical for modulation of locomotion, muscle tone, and pain responses<sup>36,37</sup>, also penetrated grafts (Fig. 4c,d).

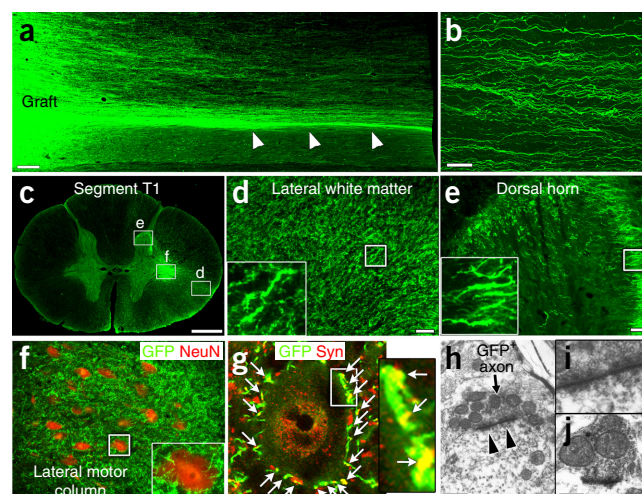


**Figure 3** Axon emergence from grafts. (a) A horizontal section of the lesion and graft site showing a large number of human, GFP-expressing axons that emerged and grew caudally in linear arrays. Many axons travel along the host white matter–gray matter interface (arrowheads). (b) Image showing the numerous linear axons present in host white matter 6 mm caudal to the lesion site. (c) A section of spinal cord segment T1, located 7 mm caudal to the lesion site, showing the large number of axons that extended into this segment. Boxed regions marked d–f are shown at higher magnification in panels d–f. (d–f) Coronal sections at T1 showing the high density of human NSC-derived axons in lateral white matter (d), superficial laminae of the dorsal horn (e), and lateral motor neuron column (f) densely surrounding ventral motor neurons. (g) Single confocal plane showing many human axon terminals on spinal motor neurons (GFP<sup>+</sup> and synaptophysin (Syn)<sup>+</sup>; arrows). Insets in d–g are a higher magnification of the smaller boxed region in each panel. (h–j) Electron micrographs from T1 ventral gray matter confirm formation of synapses (arrowheads) between GFP<sup>+</sup> human axons and host dendrites. Asymmetric synaptic morphology and circular vesicles with a dense core suggest an excitatory synapse. a, c, and d–g are from Subject 5, and b and h–j are from Subject 9. i is a higher magnification of h; j is a second example. Scale bars: a, 250  $\mu$ m; b, 20  $\mu$ m; c, 1 mm; d–f, 50  $\mu$ m; g, 10  $\mu$ m; h, 250 nm; j, 100 nm.

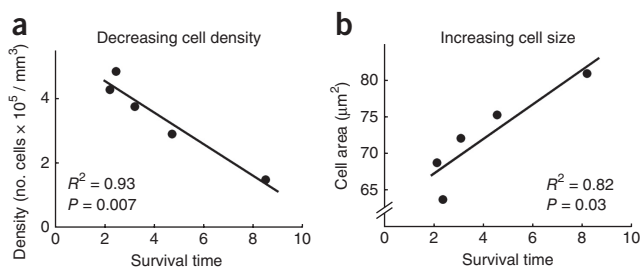


**Figure 2** Changes in graft density and cell size. (a) Graft cell density significantly declined over time ( $n = 5$  monkeys;  $P = 0.007$ , Matlab Corrcoef). (b) Mean cell size increased over time ( $n = 5$  monkeys;  $P = 0.03$ , Matlab Corrcoef).

**Table 1 Individual subject data**

Subject	Survival time (months)	Graft volume (mm <sup>3</sup> )	Graft density (cells per mm <sup>3</sup> )	Total cells (millions)	Total axons (2 mm caudal)	Cell size (μm <sup>2</sup> )
5	2	60.9	426,000	26.0	140,149	68.8
6	3	67.4	374,000	25.0	154,848	72.1
7	2	11.2	483,000	5.4	54,002	63.8
8	5	12.4	290,000	3.6	64,000	75.3
9	9	48.0	149,000	7.0	68,011	80.9

Millions of cells survived in all grafts. Up to 155,000 axons emerged from grafts at 2 mm caudal to the lesion site within 3 months of grafting. Axon numbers appeared to be stable from 5 to 9 months following grafting.

The corticospinal projection is the most important neuronal system for voluntary movement in humans, and its regeneration is likely to be important for enhancing voluntary motor movement after human SCI. Yet this is the most refractory axonal system to attempts to elicit axonal regeneration into a lesion site<sup>1</sup> (**Supplementary Fig. 9**). Recently we reported that grafts of neural stem cells driven to a spinal cord identity support regeneration of corticospinal axons in rodent models of SCI<sup>19</sup>. We now report for the first time to our knowledge the regeneration of primate corticospinal axons into human NPC grafts (**Fig. 4a,b**). Corticospinal axons readily crossed the host-graft interface to penetrate distances up to 500 μm into the graft (**Fig. 4b**).

### Functional outcomes

Monkeys were scored in an open field task that sampled over 25 features of motor function<sup>38–40</sup>. The scoring system includes several subscales for object manipulation, climbing, and overground locomotion as monkeys engage in naturalistic behaviors in a large testing enclosure<sup>38–40</sup> (**Supplementary Fig. 10**). Monkeys received points for function in each behavioral category and were given a composite score representing an overall assessment of neurological function. The primate model of C7 lesion was designed to assess potential therapies for improving distal forelimb function, as the neural circuitry for hand control is located in the C7–T1 spinal levels that range 1–20 mm below the lesion, and axons extending from a neural stem cell graft reach these segments (**Figs. 2 and 3**). Function among monkeys with non-surviving grafts (Subjects 1–4) exhibited stability or only partial spontaneous improvement up to 4–8 weeks postinjury but then reached stability without subsequent overall improvement (**Supplementary Figs. 10 and 11**), a pattern consistent with previous studies in lesion-only (untreated) control subjects<sup>27,38</sup> (**Supplementary Fig. 11**). In contrast, among monkeys with surviving grafts, the initial 4- to 8-week period of functional loss or partial spontaneous improvement after lesion was followed by a second period of subsequent improvement 10 weeks after lesion (**Supplementary Fig. 10**). Object manipulation scores recovered to >25% success in four of five monkeys with grafts but in only one of four monkeys without grafts. Moreover, peak right-hand object manipulation scores were greater in monkeys with grafts ( $P < 0.01$ , Wald chi-square; **Supplementary Fig. 10**). In contrast, the climbing score, which measures both forelimb and hindlimb use, did not differ significantly between monkeys with and without surviving grafts ( $P = 0.19$ , Wald chi-square; **Supplementary Fig. 10**). Unlike object manipulation, locomotor recovery is fairly extensive after C7 hemisection in monkeys, as in humans<sup>41</sup>, and values on this subscale differed between groups with surviving and nonsurviving grafts by only 12%, a modest amount that was nonetheless significant ( $P = 0.05$ , Wald chi-square; **Supplementary Fig. 10**). Monkeys with surviving grafts exhibited a significant degree of improvement in peak performance in an overall measure of motor function that

combines all measures as compared to monkeys without surviving grafts ( $P = 0.02$ , Wald chi-square; **Supplementary Fig. 10**).

A composite behavioral score was also generated using nonlinear principal component analysis (PCA) on functional outcome data. This demonstrated a significant difference in multidimensional recovery curves between monkeys with surviving grafts relative to those with nonsurviving grafts as determined through a last-observation-carried-forward analysis and linear mixed-model testing ( $P < 0.05$ ; **Supplementary Figs. 10 and 12**). These results are interpreted with caution because the study did not contain a lesioned control group in which no attempt to graft was made and because monkeys with poor graft survival did not live as long as monkeys with surviving grafts

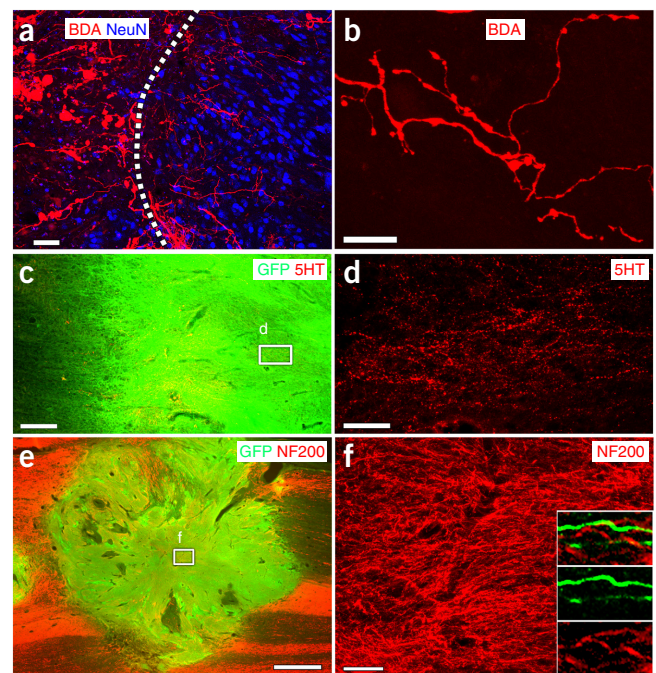


**Figure 4** Host axons regenerate into human NPC grafts. **(a)** Labelling for corticospinal axons (BDA<sup>+</sup>), which regenerate short distances (up to 500 μm) into human NPC grafts. The dashed line indicates the host-graft interface as revealed by NeuN labeling. **(b)** Image of a sample axon located 300 μm within the graft with a complex branching pattern and bouton-like swellings. **(c,d)** Serotonergic (5HT<sup>+</sup>) axons regenerate into human NPC grafts in all subjects with good rostral host-graft integration. The boxed region marked d is shown at a higher magnification in **d**. **(e,f)** Host NF200<sup>+</sup> axons extensively regenerate into NPC grafts. The boxed region marked f is shown at a higher magnification in **f**. Insets in **f**, taken in host white matter, show that graft-derived GFP<sup>+</sup> axons do not label for NF200. Scale bars: **a, b, d, and f**, 50 μm; **c**, 200 μm; **e**, 1 mm.

(Subjects 1–4 were enrolled earlier in the study, and their early euthanasia was preplanned for assessment of graft survival). However, three points support the probability that these statistically significant improvements in function in monkeys with surviving grafts reflect true recovery: (i) control lesioned animals from previous<sup>27,38</sup> and recent (**Supplementary Fig. 11**) studies did not exhibit late functional recovery of the type observed in successfully grafted monkeys; (ii) one monkey without graft survival in the present study that was perfused after 21 weeks did not show late improvement (**Supplementary Fig. 10b**); and (iii) improvements were proportionately greater in measures of forelimb than hindlimb function in successfully grafted subjects, which is consistent with dense penetration of graft-derived axons into cervical spinal cord segments (**Fig. 3**).

#### Cells do not migrate from the lesion site or form ectopic colonies

Previous studies have reported long-distance migration of human neural stem cells implanted into mouse models; this migration has consisted nearly entirely of glia<sup>42</sup>. In this study, we did not observe migration of human neurons or glia more than 100  $\mu\text{m}$  from the lesion site (**Fig. 3** and **Supplementary Fig. 1**). This result is consistent with graft-derived OLIG2<sup>+</sup> cells representing immature oligodendrocytes rather than migratory oligodendrocyte progenitor cells<sup>43</sup>. Also, ectopic deposits of grafted neural stem cells have been observed along the spinal cord central canal and on the surface of the spinal cord in rat models<sup>44,45</sup>. In the present study, we did not observe migration of implanted human neural progenitor cells in the central canal, ventricles, or brain. In one subject, a single colony of GFP-expressing NPCs was present on the spinal cord surface directly at the site of engraftment, but not at more distal sites.

Lesions in all nine monkeys were similar in extent (**Supplementary Fig. 13**). Grafts were well vascularized as revealed by both Nissl staining and collagen immunolabeling (**Supplementary Fig. 14**). Mild perivascular cellular infiltrates consisting of CD8<sup>+</sup> T cells were present in fully immunosuppressed monkeys, suggesting that there was an ongoing, low-grade immune response that continued 9 months postgrafting (**Supplementary Fig. 14**).

#### Visualization of grafts by magnetic resonance imaging

We performed high-resolution 3D T1- and T2-weighted isotropic magnetic resonance imaging (MRI) scans on a 3 Tesla Siemens clinical MR scanner in monkeys sedated with ketamine (5 mg per kg body weight) after grafting to determine whether fill of the lesion site could be detected in the living subject. Findings were compared to those from anatomical analyses (**Fig. 1** and **Supplementary Fig. 1**). Monkeys lacking surviving grafts exhibited a low signal intensity on T1-weighted imaging and a high signal intensity on T2-weighted imaging in the lesion site, whereas monkeys with surviving grafts exhibited the opposite result (**Supplementary Fig. 15**).

#### DISCUSSION

Four important observations arise from this study. First, human neural stem cells can be successfully engrafted to fill the large lesion cavity of a nonhuman primate spinal cord using methods that are unique to the primate model. These methods include an increased concentration of fibrinogen–thrombin in the grafting mixture and intraoperative drainage of CSF to create a dry grafting cavity. Second, human grafts exhibit a prolonged time period of maturation. Although the grafts continued to mature over the 9-month period of this study, functional effects of the grafts may have been evident 3–4 months postgrafting, when axons have already extended 50 mm into the

host. Immature axons and synapses conduct action potentials and are capable of influencing signal processing in the hippocampus<sup>46,47</sup>; similarly, active immature graft-derived axons could account for the functional benefits observed herein. Third, unprecedented numbers of new human axons are capable of extending out from the lesion site and into the surrounding spinal cord; up to 150,000 axons extend from the lesion on one side of the spinal cord, a substantial mass of new circuitry that represents a potential mechanism for influencing functional outcomes. Observations of functional outcomes through 9 months following SCI indicate that partial functional recovery occurs. It is possible that longer observation periods could result in greater recovery. Fourth, we describe the regeneration of corticospinal axons, essential for voluntary movement in humans, into a lesion site in a primate model for the first time to our knowledge.

Highlighting the importance of scaling up to larger animal models, we found that grafting methods that were effective in rodent models did not enable graft survival in nonhuman primates. Following several modifications to the rodent grafting technique, including modifications to the grafting matrix, physical measures (operative table tilt to drain CSF), and more extensive immunosuppression, successful engraftment was achieved. Had we or others attempted human translation without prior large animal testing, there would have been a substantial risk of clinical trial failure not because of a lack of biological therapeutic potential for neural stem cells, but as a simple result of graft loss. It is important that translational studies of invasive cellular transplantation avoid these pitfalls and utilize larger animal models when possible<sup>24,25</sup>.

A key limiting factor in the translational relevance of previous efforts to repair SCI has been limited regeneration of corticospinal axons<sup>48,49</sup>. Although enhanced sprouting of host axons in spared host gray matter after SCI through manipulation of expression of phosphatase and tensin homolog (PTEN) and suppressor of cytokine signaling 3 (SOCS3) is impressive<sup>50,51</sup>, these genetic manipulations primarily promoted corticospinal growth in spared regions of the host spinal cord rather than regeneration into spinal cord lesion sites themselves. Yet the majority of human injuries are clinically complete, and it is unclear whether targeting the relatively low number of corticospinal axons in small regions of spared host tissue will be useful<sup>52</sup>. Thus, achieving corticospinal regeneration into a lesion site is likely important in translational human therapies for severe injury<sup>53</sup>. We recently reported that spinal cord replacement with homologous spinal cord neural anlage supports corticospinal axon regeneration into lesion sites in rodents and enhances forelimb reaching function<sup>19</sup>. In the present study, primate corticospinal axons also regenerated into human neural stem cells grafted to lesion sites. Given the critical role of corticospinal systems in human fine motor control, their regeneration represents an important milestone in translational relevance of a primate model. Corticospinal axons regenerated ~0.5 mm into grafts. In future studies, we will determine whether greater distances and densities of corticospinal penetration might be achieved using therapies that enhance the endogenous growth state of host neurons, such as transient treatment with pharmacological PTEN inhibitors<sup>50,54,55</sup>.

Grafts exhibited evidence of continuing maturation over time. Astrocytes first expressed the mature marker GFAP at 5 months postgrafting, and neurons continued to exhibit increasing somal size over 9 months. The number of grafted neurons fell by approximately 50% at the longest observed time point, consistent with patterns observed in normal neural development<sup>56–58</sup>. It is possible that graft neurons that failed to form stable synapses were selectively eliminated<sup>59</sup>. It is important that future human clinical trials take into consideration

the possibility that grafts will mature gradually with potentially late effects on functional outcomes.

Finally, a major barrier to achieving adult axon regeneration has been the inhibitory nature of adult myelin against axon growth<sup>4,5</sup>. Here we show that axons emerging from human neural stem cells extend abundant axons through white matter, overcoming a major limiting factor in the regeneration field. In parallel, host adult axons regenerated into the myelin-free stem cell environment. Accordingly, neural stem cell therapy represents a means of circumventing one of the major challenges to axon regeneration in the adult CNS.

## METHODS

Methods, including statements of data availability and any associated accession codes and references, are available in the [online version of the paper](#).

*Note: Any Supplementary Information and Source Data files are available in the online version of the paper.*

## ACKNOWLEDGMENTS

Human 566RSC-UBQT neural stem cells were a gift from NeuralStem, Inc. This work was supported by the Veterans Administration (Gordon Mansfield Spinal Cord Injury Collaborative Consortium, RR&D B7332R, MHT; RR&D RX001045, JHB), the National Institutes of Health (R01 NS042291, MHT; R01 NS104442, MHT), the Department of Defense (W81XWH-12-1-0592; E.S.R.), the Craig H. Neilsen Foundation (M.H.T.), the Bernard and Anne Spitzer Charitable Trust (M.H.T.), and the Dr. Miriam and Sheldon G. Adelson Medical Research Foundation (M.H.T.).

## AUTHOR CONTRIBUTIONS

E.S.R., J.H.B., P.L., E.A.S., K.K., L.A.H., Y.S.N.-L., A.R.F., M.S.B., J.C.B., and M.H.T. designed the experiments. E.S.R., J.H.B., P.L., H.K., E.A.S., K.K., R.M., S.H., Y.S.N.-L., J.C.B., and M.H.T. carried out the experiments. E.S.R., J.H.B., H.K., E.A.S., J.L.W., J.J.L., J.R.H., L.A.H., A.R.F., and M.H.T. analyzed the data. E.S.R. and M.H.T. wrote the manuscript. E.S.R., J.H.B., P.L., H.K., E.A.S., K.K., J.L.W., J.J.L., R.M., S.H., J.R.H., L.A.H., Y.S.N.-L., A.R.F., M.S.B., J.C.B., and M.H.T. edited the manuscript.

## COMPETING INTERESTS

The authors declare no competing interests.

Reprints and permissions information is available online at <http://www.nature.com/reprints/index.html>. Publisher's note: Springer Nature remains neutral with regard to jurisdictional claims in published maps and institutional affiliations.

- Blesch, A. & Tuszynski, M.H. Spinal cord injury: plasticity, regeneration and the challenge of translational drug development. *Trends Neurosci.* **32**, 41–47 (2009).
- Fawcett, J.W. Overcoming inhibition in the damaged spinal cord. *J. Neurotrauma* **23**, 371–383 (2006).
- Fitch, M.T. & Silver, J. CNS injury, glial scars, and inflammation: inhibitory extracellular matrices and regeneration failure. *Exp. Neurol.* **209**, 294–301 (2008).
- He, Z. & Koprivica, V. The Nogo signaling pathway for regeneration block. *Annu. Rev. Neurosci.* **27**, 341–368 (2004).
- Schwab, M.E. Nogo and axon regeneration. *Curr. Opin. Neurobiol.* **14**, 118–124 (2004).
- Lu, P. & Tuszynski, M.H. Growth factors and combinatorial therapies for CNS regeneration. *Exp. Neurol.* **209**, 313–320 (2008).
- Filbin, M.T. Recapitulate development to promote axonal regeneration: good or bad approach? *Phil. Trans. R. Soc. Lond. B* **361**, 1565–1574 (2006).
- Kadoya, K. *et al.* Combined intrinsic and extrinsic neuronal mechanisms facilitate bridging axonal regeneration one year after spinal cord injury. *Neuron* **64**, 165–172 (2009).
- Jakeman, L.B. & Reier, P.J. Axonal projections between fetal spinal cord transplants and the adult rat spinal cord: a neuroanatomical tracing study of local interactions. *J. Comp. Neurol.* **307**, 311–334 (1991).
- Reier, P.J., Stokes, B.T., Thompson, F.J. & Anderson, D.K. Fetal cell grafts into resection and contusion/compression injuries of the rat and cat spinal cord. *Exp. Neurol.* **115**, 177–188 (1992).
- Wictorin, K. & Björklund, A. Axon outgrowth from grafts of human embryonic spinal cord in the lesioned adult rat spinal cord. *Neuroreport* **3**, 1045–1048 (1992).
- Coumans, J.V. *et al.* Axonal regeneration and functional recovery after complete spinal cord transection in rats by delayed treatment with transplants and neurotrophins. *J. Neurosci.* **21**, 9334–9344 (2001).
- Cummings, B.J. *et al.* Human neural stem cells differentiate and promote locomotor recovery in spinal cord-injured mice. *Proc. Natl. Acad. Sci. USA* **102**, 14069–14074 (2005).
- Salazar, D.L., Uchida, N., Hamers, F.P.T., Cummings, B.J. & Anderson, A.J. Human neural stem cells differentiate and promote locomotor recovery in an early chronic spinal cord injury NOD-scid mouse model. *PLoS One* **5**, e12272 (2010).
- Bonner, J.F. *et al.* Grafted neural progenitors integrate and restore synaptic connectivity across the injured spinal cord. *J. Neurosci.* **31**, 4675–4686 (2011).
- Courtine, G. *et al.* Recovery of supraspinal control of stepping via indirect propriospinal relay connections after spinal cord injury. *Nat. Med.* **14**, 69–74 (2008).
- Lu, P. *et al.* Long-distance growth and connectivity of neural stem cells after severe spinal cord injury. *Cell* **150**, 1264–1273 (2012).
- Lu, P. *et al.* Long-distance axonal growth from human induced pluripotent stem cells after spinal cord injury. *Neuron* **83**, 789–796 (2014).
- Kadoya, K. *et al.* Spinal cord reconstitution with homologous neural grafts enables robust corticospinal regeneration. *Nat. Med.* **22**, 479–487 (2016).
- Rosenzweig, E.S. *et al.* Extensive spinal decussation and bilateral termination of cervical corticospinal projections in rhesus monkeys. *J. Comp. Neurol.* **513**, 151–163 (2009).
- Kuypers, H.G.J.M. in *Handbook of Physiology* (eds. Brooks, V.B., Brookhart, J.M. & Mountcastle, V.B.). Anatomy of the descending pathways (The American Physiological Society, 1981).
- Lacroix, S. *et al.* Bilateral corticospinal projections arise from each motor cortex in the macaque monkey: a quantitative study. *J. Comp. Neurol.* **473**, 147–161 (2004).
- Galea, M.P. & Darian-Smith, I. Manual dexterity and corticospinal connectivity following unilateral section of the cervical spinal cord in the macaque monkey. *J. Comp. Neurol.* **381**, 307–319 (1997).
- Kwon, B.K. *et al.* Large animal and primate models of spinal cord injury for the testing of novel therapies. *Exp. Neurol.* **269**, 154–168 (2015).
- Tuszynski, M.H. in *Translational Neuroscience* 1st edn. (ed. Tuszynski, M.H.) Conclusion (Springer US, 2016).
- Anderson, A.J., Piltti, K.M., Hooshmand, M.J., Nishi, R.A. & Cummings, B.J. Preclinical efficacy failure of human CNS-derived stem cells for use in the pathway study of cervical spinal cord injury. *Stem Cell Rep.* **8**, 249–263 (2017).
- Rosenzweig, E.S. *et al.* Extensive spontaneous plasticity of corticospinal projections after primate spinal cord injury. *Nat. Neurosci.* **13**, 1505–1510 (2010).
- Cizkova, D. *et al.* Functional recovery in rats with ischemic paraplegia after spinal grafting of human spinal stem cells. *Neuroscience* **147**, 546–560 (2007).
- Guo, X., Johe, K., Molnar, P., Davis, H. & Hickman, J. Characterization of a human fetal spinal cord stem cell line, NSI-566RSC, and its induction to functional motoneurons. *J. Tissue Eng. Regen. Med.* **4**, 181–193 (2010).
- Glass, J.D. *et al.* Lumbar intraspinal injection of neural stem cells in patients with amyotrophic lateral sclerosis: results of a phase I trial in 12 patients. *Stem Cells* **30**, 1144–1151 (2012).
- Sun, W. *et al.* SOX9 is an astrocyte-specific nuclear marker in the adult brain outside the neurogenic regions. *J. Neurosci.* **37**, 4493–4507 (2017).
- Ren, Y. *et al.* Ependymal cell contribution to scar formation after spinal cord injury is minimal, local and dependent on direct ependymal injury. *Sci. Rep.* **7**, 41122 (2017).
- Golan, N. *et al.* Identification of Tmem10/Opalin as an oligodendrocyte enriched gene using expression profiling combined with genetic cell ablation. *Glia* **56**, 1176–1186 (2008).
- Lu, P. *et al.* Prolonged human neural stem cell maturation supports recovery in injured rodent CNS. *J. Clin. Invest.* **127**, 3287–3299 (2017).
- Custo Greig, L.F., Woodworth, M.B., Galazo, M.J., Padmanabhan, H. & Macklis, J.D. Molecular logic of neocortical projection neuron specification, development and diversity. *Nat. Rev. Neurosci.* **14**, 755–769 (2013).
- Fields, H.L., Heinricher, M.M. & Mason, P. Neurotransmitters in nociceptive modulatory circuits. *Annu. Rev. Neurosci.* **14**, 219–245 (1991).
- Schmidt, B.J. & Jordan, L.M. The role of serotonin in reflex modulation and locomotor rhythm production in the mammalian spinal cord. *Brain Res. Bull.* **53**, 689–710 (2000).
- Nout, Y.S. *et al.* Methods for functional assessment after C7 spinal cord hemisection in the rhesus monkey. *Neurorehabil. Neural Repair* **26**, 556–569 (2012).
- Nout, Y.S. *et al.* Animal models of neurologic disorders: a nonhuman primate model of spinal cord injury. *Neurotherapeutics* **9**, 380–392 (2012).
- Salegio, E.A. *et al.* A unilateral cervical spinal cord contusion injury model in non-human primates (*Macaca mulatta*). *J. Neurotrauma* **33**, 439–459 (2016).
- Friedli, L. *et al.* Pronounced species divergence in corticospinal tract reorganization and functional recovery after lateralized spinal cord injury favors primates. *Sci. Transl. Med.* **7**, 302ra134 (2015).
- Windrem, M.S. *et al.* Fetal and adult human oligodendrocyte progenitor cell isolates myelinate the congenitally dysmyelinated brain. *Nat. Med.* **10**, 93–97 (2004).
- Osorio, M.J. & Goldman, S.A. Glial progenitor cell-based treatment of the childhood leukodystrophies. *Exp. Neurol.* **283** Part B, 476–488 (2016).

44. Steward, O., Sharp, K.G., Yee, K.M., Hatch, M.N. & Bonner, J.F. Characterization of ectopic colonies that form in widespread areas of the nervous system with neural stem cell transplants into the site of a severe spinal cord injury. *J. Neurosci.* **34**, 14013–14021 (2014).
45. Tuszynski, M.H. *et al.* Neural stem cell dissemination after grafting to CNS injury sites. *Cell* **156**, 388–389 (2014).
46. Mongiat, L.A., Espósito, M.S., Lombardi, G. & Schinder, A.F. Reliable activation of immature neurons in the adult hippocampus. *PLoS One* **4**, e5320 (2009).
47. Dieni, C.V. *et al.* Low excitatory innervation balances high intrinsic excitability of immature dentate neurons. *Nat. Commun.* **7**, 11313 (2016).
48. Hollis, E.R. II., Jamshidi, P., Löw, K., Blesch, A. & Tuszynski, M.H. Induction of corticospinal regeneration by lentiviral trkB-induced Erk activation. *Proc. Natl. Acad. Sci. USA* **106**, 7215–7220 (2009).
49. Ghosh, M. *et al.* Extensive cell migration, axon regeneration, and improved function with polysialic acid-modified Schwann cells after spinal cord injury. *Glia* **60**, 979–992 (2012).
50. Liu, K. *et al.* PTEN deletion enhances the regenerative ability of adult corticospinal neurons. *Nat. Neurosci.* **13**, 1075–1081 (2010).
51. Jin, D. *et al.* Restoration of skilled locomotion by sprouting corticospinal axons induced by co-deletion of PTEN and SOCS3. *Nat. Commun.* **6**, 8074 (2015).
52. Tuszynski, M.H., Gabriel, K., Gerhardt, K. & Szollar, S. Human spinal cord retains substantial structural mass in chronic stages after injury. *J. Neurotrauma* **16**, 523–531 (1999).
53. Lu, P., Ahmad, R. & Tuszynski, M.H. in *Translational Neuroscience* 1st edn. (ed. Tuszynski, M.H.) Neural Stem Cells for Spinal Cord Injury (Springer US, 2016).
54. Christie, K.J., Webber, C.A., Martinez, J.A., Singh, B. & Zochodne, D.W. PTEN inhibition to facilitate intrinsic regenerative outgrowth of adult peripheral axons. *J. Neurosci.* **30**, 9306–9315 (2010).
55. Schmid, A.C., Byrne, R.D., Vilar, R. & Woscholski, R. Bisperoxovanadium compounds are potent PTEN inhibitors. *FEBS Lett.* **566**, 35–38 (2004).
56. Raff, M.C. *et al.* Programmed cell death and the control of cell survival: lessons from the nervous system. *Science* **262**, 695–700 (1993).
57. Raff, M.C. Size control: the regulation of cell numbers in animal development. *Cell* **86**, 173–175 (1996).
58. Jacobson, M.D., Weil, M. & Raff, M.C. Programmed cell death in animal development. *Cell* **88**, 347–354 (1997).
59. Maor-Nof, M. & Yaron, A. Neurite pruning and neuronal cell death: spatial regulation of shared destruction programs. *Curr. Opin. Neurobiol.* **23**, 990–996 (2013).

## ONLINE METHODS

**Subjects.** We studied a total of nine male rhesus macaques (*Macaca mulatta*) aged 6–10 years that had not participated in any previous studies. *Post hoc* anatomical analyses separated the subjects into two groups according to graft survival ( $n = 4$  monkeys without grafts;  $n = 5$  monkeys with grafts). Our previous work in this model of SCI has demonstrated sufficiently low variability to achieve statistical significance with groups of this size<sup>27</sup>. All surgical and experimental procedures adhered to the principles outlined by the American Association for the Accreditation of Laboratory Animal Care and were approved by the Institutional Animal Care and Use Committee (IACUC) at the California National Primate Research Center (Davis, CA). Subjects were housed at the California National Primate Research Center (Davis, CA), and surgeries were performed there. Subsequent tissue processing and analysis was performed at the Center for Neural Repair (University of California, San Diego, La Jolla, CA).

**Lesion surgery.** Monkeys were sedated with 1 mg ketamine per kg body weight intramuscularly and anesthetized with 1.5–2.5% isoflurane. The caudal half of the C5 dorsal lamina and the entire C6 dorsal lamina were removed. The dura was slit longitudinally along the midline and retracted gently. A surgical microknife was mounted on a stereotaxic arm positioned at the spinal midline midway between the C5 and C6 dorsal laminae. This rostro-caudal position corresponds to the C7 spinal cord segment. The stereotaxic manipulator was used to lower the blade through the entire dorsoventral extent of the spinal cord without severing the ventral artery. This initial cut established the medial position of the lesion. The surgeon then used micro-scissors to complete the lesion using microscopic observation to ensure lateral and ventral lesion completeness. Monkeys retained bowel, bladder, and autonomic function after SCI. Lesion reconstructions are shown in **Supplementary Figure 13**.

**Immunosuppression.** All grafted subjects received a triple-therapy immunosuppressive regimen comprising mycophenolate mofetil (MMF; CellSept), tacrolimus (FK-506; ProGraf), and prednisone. Treatment began 1 d before grafting, and drugs were administered orally or through a nasogastric tube. In all subjects, the initial dose of prednisone was 2 mg per kg body weight per day and was reduced to 1 mg per kg body weight per day on the second day after transplantation. In Subjects 1–4, the initial dosage of MMF was 50 mg per kg body weight per day, and the initial dosage of FK-506 was 0.3 mg per kg per body weight per day. Treatment with both drugs was split into 2 doses (a.m. and p.m.). Initial dosages of MMF and FK-506 were increased to 100 mg per kg body weight per day and 1 mg per kg body weight per day, respectively, owing to poor graft survival in Subjects 1–4. Blood trough levels of MMF (target range, 3–6 µg/ml) and FK-506 (target range, 4–10 ng/ml) were assessed 1–3 times per week to adjust dosages. Immunosuppression continued until date of euthanization.

**Grafting.** Two weeks after the C7 right lateral hemisection, we grafted 20 million GFP-expressing human neural progenitor cells into the lesion site. This karyotypically stable cell line (566RSC-UBQT) was derived from the lower cervical and upper thoracic spinal cord of an 8-week-old fetus that was donated in accordance with National Institutes of Health and Food and Drug Administration guidelines<sup>28</sup>. As previously reported<sup>29,30</sup>, the vast majority (94%) of these cells express nestin and are uncommitted to neuronal or glial lineage before transplantation. These cells are maintained, authenticated, and tested for mycoplasma by NeuralStem, Inc. Human NPCs were shipped at 4 °C while suspended at 20,000 cells per µl of a proprietary hibernation medium with overnight delivery. Subjects were sedated and anesthetized as described above, and the lesion site was re-exposed. Hibernation media were removed, and then human NPCs were suspended at 200,000 cells per µl of a two-part fibrin matrix (human fibrinogen, Sigma, F3879, 100 mg/ml; human thrombin, Sigma, T7009, 100 U/ml) containing a cocktail of growth factors: brain-derived neurotrophic factor (BDNF; 50 µg/ml, Peprotech, 452-02), neurotrophin-3 (NT-3; 50 µg/ml, Peprotech, 450-03), glial-cell-line-derived neurotrophic factor (GDNF; 10 µg/ml, Sigma, G1401), epidermal growth factor (EGF; 10 µg/ml, Sigma, E1257), basic fibroblast growth factor (bFGF; 10 µg/ml, Sigma, F0291), acidic fibroblast growth factor (aFGF; 10 µg/ml, Sigma, F5542), hepatocyte growth factor (HGF; 10 µg/ml, Sigma, H9661), insulin-like growth factor 1 (IGF-1; 10 µg/ml,

Sigma, I8779), platelet-derived growth factor (PDGF-AA; 10 µg/ml, Peprotech, 100-13A), vascular endothelial growth factor (VEGF; 10 µg/ml; Peprotech, 100-20), and a calpain inhibitor (MDL28170; 50 µM, Sigma, M6690). For Subjects 3–9, immediately before the placement of cells into the lesion site, the surgical table was tilted to an approximately 30° angle (head upward). This temporarily drains CSF away from the lesion site, providing 5–15 min for surgeons to place the cells and for the liquid components of the fibrin matrix to form a gel that held the NPCs in the lesion site. After the gel formed, the dura, muscles and fascia, and skin were sutured closed in layers.

**Corticospinal tracing.** Corticospinal tract (CST) axons were traced in Subject 9 to assess regeneration into the graft. As previously described<sup>20</sup>, 6 weeks before euthanization, the subject was anesthetized and a craniotomy was performed to expose the left motor cortex. 300 nl of the anterograde neuronal tracer biotinylated dextran amine (BDA; 10,000 molecular weight, 10% in water; Thermo Fisher) was injected at each of 127 sites (59 different surface locations). These sites included motor cortex innervating regions of spinal cord controlling the hand, arm, trunk, leg, and foot.

**Tissue processing.** Subjects were euthanized 2–9 months after receiving human NPC grafts. Subjects were deeply anesthetized and transcardially perfused with a 4% solution of paraformaldehyde, and the spinal cord was dissected out of the spinal column. Spinal cord dura was removed, and the spinal cord was cut in the transverse plane into 1- or 1.5-cm-long blocks as described previously<sup>27</sup>. The block containing the lesion was cut into 30-µm-thick horizontal sections using a freezing microtome. Additional blocks of tissue were cut into 40-µm-thick transverse sections. In Subject 9, the tissue blocks immediately rostral and caudal to the lesion block were first partially cut (6 transverse sections that were 50 µm thick) using a vibratome; this method is more compatible with electron microscopy. The vibratome-cut sections were then immediately immunolabeled for green fluorescent protein (see below), and the remaining tissue in those blocks was cut on a microtome in the same fashion as the other spinal cords. Tissue sections were stored at –20 °C in tissue cryoprotectant solution (TCS; 25% glycerin (vol/vol) and 30% ethylene glycol (vol/vol) in 0.5 M phosphate buffer).

**Fluorescent immunolabeling.** Transverse sections were pretreated with 50% methanol for 20 min at 22–24 °C, washed in Tris-buffered saline (TBS) and blocked for 1 h in TBS containing 5% normal donkey serum and 0.25% Triton X-100. Sections were incubated in primary antibodies against GFP (rabbit, Thermo Fisher no. 6455, 1:1,500); GFAP (chicken, Encor Bio no. CPCA-GFAP, 1:1,500, to label astrocytes); NeuN (mouse, Millipore MAB377, 1:1,000, to label mature neurons); class III β-tubulin (mouse, Promega G-7121, 1:1,000, to label immature and mature neurons); neurofilament light-chain (NF70, mouse, Millipore MAB1615, 1:300, to label immature axons); neurofilament unphosphorylated heavy-chain (SMI32, mouse, Covance no. SMI-32P, 1:2,000); neurofilament phosphorylated heavy-chain (NF200, mouse, Millipore MAB5262, 1:500); Ki-67 (rabbit, Abcam ab1666, 1:250, to label dividing cells); OLIG2 (rabbit, IBL no. 18953, 1:200, to label oligodendrocytes and MN precursors); OPALIN (mouse, Santa Cruz Biotechnology no. sc-374490, 1:200, to label myelinating oligodendrocytes); SOX9 (goat, R&D Systems no. AF3075, 1:1,000, to label astrocytes and ependymal cells); and HOMER1 (rabbit, Synaptic Systems no. 160003, 1:1,000, to label postsynaptic densities). BDA was detected with Alexa-Fluor 594- or Alexa-Fluor 568-conjugated streptavidin (Thermo Fisher S11226, 1:1,000). Sections were washed with TBS and then incubated in Alexa-Fluor 488- or Alexa-Fluor 594-conjugated anti-goat or anti-donkey secondary antibodies (Thermo Fisher A11055, A11058, SA5-10062, SA5-10064, 1:500) for 1 h and DAPI (Sigma D9542, 0.5 µg/µl, to label nuclei) for 5 min. Sections were washed with TBS, mounted on slides, and coverslipped with Mowiol mounting medium (<http://cshprotocols.cshlp.org/content/2006/1/pdb.rec10255>). All antibodies were used previously in monkeys and/or on the 566RSC-UBQT cell line<sup>17,27,28</sup>.

**Electron microscopy.** Some tissue sections from Subject 9 were analyzed with a combination of immunolabeling (for GFP) and electron microscopy (to identify synaptic structures). Sections were postfixed for 1 h in 0.1% glutaraldehyde in 0.1 M phosphate buffer (PB), and then endogenous peroxidase



activity was quenched in 0.6% H<sub>2</sub>O<sub>2</sub> in TBS for 30 min. Sections were permeabilized in 50% ethanol in TBS for 30 min, incubated in 1% sodium borohydride in TBS for 30 min, and blocked in 5% horse serum and 0.025% Triton X-100 in TBS for 1 h. Sections were incubated for 3 nights in primary antibody (rabbit anti-GFP, Thermo Fisher no. A6455, 1:3,000 in blocking buffer). Sections were then incubated for 1 h in Vector Impress Poly-HRP secondary antibody (Vector no. MP-7401, 1:1 in TBS). Finally, a visible reaction product was developed in 0.05% diaminobenzidine, 0.04% nickel chloride, and 0.012% H<sub>2</sub>O<sub>2</sub> in TBS for approximately 4 min. Wet sections were next examined by light microscopy, and the portions containing visible reaction products within the spinal cord gray matter were trimmed and processed for ultrastructural studies. The trimmed sections were first immersed in a 1% osmium tetroxide solution (Ted Pella, Inc.), dehydrated in a graded series of ethanol, and immersed in 100% propylene oxide. Sections were next embedded in an epoxy resin using the Eponate 12 kit with DMP-30 as an accelerator (Ted Pella, Inc. no. 18010). Ultrathin sections were cut with thickness of 60–70 nm using an RMC Products PowerTome Ultramicrotome (Boeckeler Instruments), and the ultrathin sections were collected on formvar-coated one-hole copper grids. The sections were contrasted with uranyl acetate and lead citrate. The ultrathin sections were finally examined in a JEOL 100 CX transmission electron microscope. Neuronal processes containing electron-dense reaction products were photographed at a magnification of 7,200 $\times$ , and images were captured on an electron microscope film (Electron Microscopy Sciences).

**Image acquisition.** Epifluorescent images were captured using an Optronics Microfire A/R digital camera (<http://www.optronics.com>) or a Keyence BZ-X710 all-in-one microscope and camera. Confocal images were captured with an Olympus Fluoview FV1000 confocal microscope (<http://www.olympusamerica.com>) set for sequential scanning. For publication, images were processed uniformly for optimal brightness and contrast using Adobe Photoshop CS5 (Adobe Systems, San Jose, CA). Images intended for quantification (see below) were not modified in this fashion. Composites of multiple focal planes were constructed either in Adobe Photoshop CS5 or ImageJ 1.48v (Wayne Rasband, National Institutes of Health; <http://rsb.info.nih.gov/ij/>).

**Quantification of graft volume, neural cell density, and axon number.** Graft-derived cells were quantified in confocal image stacks by counting individual cells labeled with GFP and NeuN within a fixed rectangular region of interest (ROI) drawn with ImageJ. All cells within the ROI were counted, and the area was quantified. For each monkey, 5–14 image stacks (spread in a grid across the graft) were quantified (a mean of 766  $\pm$  100 individual cells per subject). Cell density was estimated via dividing the number of cells by the ROI volume. Additional estimates of the proportion of cells in the graft coexpressing NeuN, OLIG2, SOX9, or Ki-67 were made under epifluorescent illumination using StereoInvestigator (MicroBrightfield, <http://www.mbfioscience.com>). Graft area was measured in horizontal tissue sections (1:12 series; a mean of 14.4  $\pm$  0.9 sections per monkey) under epifluorescent illumination using StereoInvestigator. Graft volume was estimated as (summed area across all sections)  $\times$  (average section thickness)  $\times$  (inverse of the sampling frequency).

Total graft-derived cell counts were estimated through multiplying the cell density by the graft volume. The number of GFP-labeled axons was quantified under epifluorescent illumination using StereoInvestigator (MicroBrightfield; <http://www.mbfioscience.com>). In horizontal tissue sections (1:12 series), a transverse line was drawn 2 mm caudal to the edge of the graft using a 4 $\times$  objective. Axons that intersected the line were marked and counted using a 60 $\times$  objective, and the total axon number per subject was estimated by multiplying the axon count by the inverse of the sampling frequency.

**Functional testing.** Functional recovery was evaluated weekly throughout the study in an open-field task previously developed by our group to assess general motor function and overground locomotion, climbing and object manipulation<sup>38–40</sup>. Behavioral assessments in this open field were typically performed live with two observers: one videotaping the session (R.M. or S.H.), and one recording behavioral observations on the scoring sheet (E.S. or J.C.B.). Alternatively, sessions were scored directly from the video; the videos were also used to

confirm live scoring results. Inter-rater reliability was evaluated periodically, and high levels of agreement were obtained (E.S. and J.C.B.). All assessments were performed without knowledge of group inclusion, as the observers had no way of knowing which monkeys had surviving transplants. Monkeys entered an open field testing enclosure (10 feet long  $\times$  6 feet wide  $\times$  7 feet high) and had access to four ascending perches to reach a food reward placed inside a Kong (a hollow rubber toy filled with raisins, apple pieces, peanuts, dry fruit, etc.; Kong Co., Golden CO) positioned on the highest perch. Locomotor activity was evaluated while the monkeys traversed the perches as well as the floor of the open cage. Climbing was assessed during retrieval of similar food objects placed in cups hanging at various heights (1.5, 2.7, 3.5, 4.3, and 4.7 feet) along the front of the cage. Object manipulation was assessed during manipulation of the Kong toy and during the consumption of a large food item to encourage bimanual manipulation (for example, an apple or orange; see **Supplementary Fig. 10**). A modified 72-point scale was used and assigned points for behavioral function. The object manipulation subscale had 22 points and was used to assess forelimb function while manipulating objects and to score posture, method used to support object (i.e., volar versus nonvolar surface of hand), joint and finger movements, digit 1 opposition, and pincer grasp. We compared the level of functional performance of monkeys with surviving grafts ( $n = 5$ ) and nonsurviving grafts ( $n = 4$ ). Because groups were established after euthanization, experimenters were blind to group membership. Although monkeys survived for differing lengths of time after grafting, the performance of all monkeys reached an asymptote during their survival period (**Supplementary Fig. 10**), as assessed by modified moving averages. Accordingly, we calculated the maximal score for each monkey during the period of asymptotic function (see **Supplementary Figs. 10–12**).

**Statistical analysis and reproducibility.** All immunohistochemical reactions were performed at least twice with similar results. Graft cell densities, sizes, and axon counts were analyzed with Matlab 2010b (MathWorks). The ‘Corrcoef’ function was used to calculate the correlation ( $R^2$ ) of these variables with survival time and the  $P$  values of those correlations. Functional data were analyzed by applied biostatisticians (J.R.H. and A.R.F.) who were blinded to experimental conditions. Nonparametric tests on single (univariate) outcome measures were executed using generalized linear modeling (GZLM), and significance was assessed using the Wald chi-square test. To assess the multivariate effect of behavioral outcome measures, we integrated these data using a modern data-driven analytics approach in which a combined behavioral endpoint was derived through a multidimensional pattern detector (nonlinear principal-component analysis; NL-PCA) in an unsupervised manner and blinded to experimental condition. Our analytical workflow involved two distinct stages of statistical analysis (**Supplementary Fig. 12**): stage 1, multidimensional endpoint description using PCA and validation of PC loading patterns; and stage 2, hypothesis testing using the validated multidimensional pattern (PC1) as the primary combinatorial endpoint. Stage 1 pattern detection was assessed using multidimensional endpoint variable integration into PC1, which was followed by examination of variance explained and PC loadings for statistical and face validity, respectively. Once that single, PCA-weight-combined endpoint axis (PC1) was deemed reproducible and valid, we applied the PC weights to derive the unique PC score for each monkey at each time point and rigorously validated these using previously established statistical decision rules<sup>60–63</sup>. The PC scores were then plotted over time, and if a monkey’s recovery time did not reach 21 weeks, the last observed PC score for that monkey was carried forward to 21 weeks using techniques consistent with best practices from the clinical literature<sup>64</sup>. Only after PC scores were mathematically derived for each subject and time point (**Supplementary Fig. 12a–c**) did we move to the stage 2 hypothesis testing (**Supplementary Fig. 12d,e**). Hypothesis testing used PC scores as the primary endpoint to assess impact of graft condition on behavioral outcome. A linear mixed model (LMM; IBM SPSS ‘Mixed’ subcommand) was then applied to assess group differences in PC1 scores over time. This variance components approach is resistant to errors caused by missing data and independence violations that would otherwise undermine the validity of repeated-measures ANOVA in this context. Prior work from our group and others have demonstrated that PCA is robust and stable when used in this context (even with a small sample size)<sup>27,41</sup> as long as the variance explained by

PC1 is high and the communalities are high. These statistical features indicate that the combined information provided by the optimally weighted combination of variables (PC1) is greater than the sum of the raw endpoint variables regardless of sample size<sup>62</sup>. The statistical analysis plan was carried out by the project's independent statistical analysis core (blinded to treatment until the final analysis step). The goal was to maximize information gain in the most transparent and statistically appropriate manner given the costs and the desire to limit subject numbers in primate studies<sup>65</sup>. All analyses were carried out in SPSS v.23 (IBM). PC loadings were considered significant at  $|0.4|$ . Significance for GZLM and LMM was assessed at  $P < 0.05$ .

**Life Sciences Reporting Summary.** Further information on experimental design and reagents is available in the **Life Sciences Reporting Summary**.

**Data availability.** The data that support the findings of this study are available from the corresponding author upon reasonable request.

60. Kaiser, H.F. Directional statistical decisions. *Psychol. Rev.* **67**, 160–167 (1960).
61. Cattell, R.B. The scree test for the number of Factors. *Multivariate Behav. Res.* **1**, 245–276 (1966).
62. Guadagnoli, E. & Velicer, W.F. Relation of sample size to the stability of component patterns. *Psychol. Bull.* **103**, 265–275 (1988).
63. Ferguson, A.R. *et al.* Derivation of multivariate syndromic outcome metrics for consistent testing across multiple models of cervical spinal cord injury in rats. *PLoS One* **8**, e59712 (2013).
64. Little, R.J.A. & Rubin, D.B. *Statistical Analysis with Missing Data* 2nd edn (John Wiley & Sons, Inc., 2002).
65. Bacchetti, P., Deeks, S.G. & McCune, J.M. Breaking free of sample size dogma to perform innovative translational research. *Sci. Transl. Med.* **3**, 87ps24 (2011).

## Life Sciences Reporting Summary

Nature Research wishes to improve the reproducibility of the work that we publish. This form is intended for publication with all accepted life science papers and provides structure for consistency and transparency in reporting. Every life science submission will use this form; some list items might not apply to an individual manuscript, but all fields must be completed for clarity.

For further information on the points included in this form, see [Reporting Life Sciences Research](#). For further information on Nature Research policies, including our [data availability policy](#), see [Authors & Referees](#) and the [Editorial Policy Checklist](#).

Please do not complete any field with "not applicable" or n/a. Refer to the help text for what text to use if an item is not relevant to your study. For final submission: please carefully check your responses for accuracy; you will not be able to make changes later.

### ▶ Experimental design

#### 1. Sample size

Describe how sample size was determined.

This study did not have an a priori control group, as we originally set out to establish procedures for grafting into primate SCI. The number of subjects without surviving grafts was established post-hoc. Our previous results in other primate studies suggest that the final group sizes (N=5 graft, 4 control) are sufficient to detect group differences, especially when combined with principal components analysis (when the analysis detects a PC1 with a high explained variance, as is the case here).

#### 2. Data exclusions

Describe any data exclusions.

No data were excluded from the analysis.

#### 3. Replication

Describe the measures taken to verify the reproducibility of the experimental findings.

We describe herein all 9 subjects that received grafts of the 566-RSC cell line. As noted in the text, the first 4 grafts failed to survive / integrate with the host spinal cord. The following 5 subjects were all successful, as shown in Fig. 1 and Suppl. Fig 1. In addition, as now noted in 'Statistics and reproducibility', All immunohistochemical reactions were performed at least twice with similar results.

#### 4. Randomization

Describe how samples/organisms/participants were allocated into experimental groups.

Histological analyses of graft survival determined group membership.

#### 5. Blinding

Describe whether the investigators were blinded to group allocation during data collection and/or analysis.

Functional data were acquired and analyzed in a blinded fashion, as there was not an a priori control group. Histological analyses of graft survival determined group membership. Anatomical quantification was limited to subjects with surviving grafts, therefore group membership was not applicable.

Note: all in vivo studies must report how sample size was determined and whether blinding and randomization were used.

## 6. Statistical parameters

For all figures and tables that use statistical methods, confirm that the following items are present in relevant figure legends (or in the Methods section if additional space is needed).

n/a Confirmed

- The exact sample size ( $n$ ) for each experimental group/condition, given as a discrete number and unit of measurement (animals, litters, cultures, etc.)
- A description of how samples were collected, noting whether measurements were taken from distinct samples or whether the same sample was measured repeatedly
- A statement indicating how many times each experiment was replicated
- The statistical test(s) used and whether they are one- or two-sided  
*Only common tests should be described solely by name; describe more complex techniques in the Methods section.*
- A description of any assumptions or corrections, such as an adjustment for multiple comparisons
- Test values indicating whether an effect is present  
*Provide confidence intervals or give results of significance tests (e.g.  $P$  values) as exact values whenever appropriate and with effect sizes noted.*
- A clear description of statistics including central tendency (e.g. median, mean) and variation (e.g. standard deviation, interquartile range)
- Clearly defined error bars in all relevant figure captions (with explicit mention of central tendency and variation)

*See the web collection on [statistics for biologists](#) for further resources and guidance.*

## ► Software

Policy information about [availability of computer code](#)

### 7. Software

Describe the software used to analyze the data in this study.

StereoInvestigator and NIH ImageJ were used for image analysis as described in Methods. Adobe Photoshop CS5 was used for image brightness and contrast adjustment. SPSS v.23 and Matlab 2010b were used for statistical analyses as described in Methods.

For manuscripts utilizing custom algorithms or software that are central to the paper but not yet described in the published literature, software must be made available to editors and reviewers upon request. We strongly encourage code deposition in a community repository (e.g. GitHub). [Nature Methods guidance for providing algorithms and software for publication](#) provides further information on this topic.

## ► Materials and reagents

Policy information about [availability of materials](#)

### 8. Materials availability

Indicate whether there are restrictions on availability of unique materials or if these materials are only available for distribution by a third party.

566-RSC cells were a gift from NeuralStem, Inc. Requests for aliquots of these cells should be directed toward that company.

## 9. Antibodies

Describe the antibodies used and how they were validated for use in the system under study (i.e. assay and species).

Antibody validation:

GFP (rabbit, Thermo Fisher #6455, 1:1500): Manufacturer's website lists reactivity in human, 23 references documenting use in immunohistochemistry.

GFAP (chicken, Encor Bio #CPCA-GFAP, 1:1500); Manufacturer's website lists reactivity in human, use in immunohistochemistry in 4 references, including the original 1972 paper (Bignami et al., Brain Res).

NeuN (mouse, Millipore MAB377, 1:1000); Manufacturer's website lists reactivity in human, use in immunohistochemistry in >50 references.

$\beta$ III Tubulin (mouse, Promega G-7121, 1:1000); Manufacturer's website lists reactivity in most mammalian species, use in immunohistochemistry in 6 references.

Neurofilament light-chain (NF70, mouse, Millipore MAB1615, 1:300); Manufacturer's website lists reactivity in human, use in immunohistochemistry in 20 references.

Neurofilament unphosphorylated heavy-chain (SMI32, mouse, Covance #SMI-32P, now owned by BioLegend, 1:2000); Manufacturer's website lists reactivity in human, use in immunohistochemistry in 4 references.

Neurofilament phosphorylated heavy-chain (NF200, mouse, Millipore MAB5262, 1:500); Manufacturer's website lists reactivity in human, use in immunohistochemistry in 16 references. In addition, we demonstrate in Suppl. Fig. 6 successful use of this antibody to label human axons.

Ki-67 (rabbit, Abcam #ab1666, 1:250); Manufacturer's website lists reactivity in human, use in 372 references, including many immunohistochemistry applications.

Olig2 (rabbit, IBL #18953, 1:200); Manufacturer's website lists reactivity in human, use in immunohistochemistry in 6 references.

Opalin (mouse, Santa Cruz Biotechnology #sc-374490, 1:200); Manufacturer's website lists reactivity in human, use in immunohistochemistry in 7 references. Opalin's use as a label for myelinating oligodendrocytes was demonstrated by Golan, Adamsky, et al. (Glia, 2008). In addition, we demonstrate in Suppl. Fig. 2 successful use of this antibody to label myelinating oligodendrocytes.

Sox9 (goat, R&D Systems #AF3075, 1:1000); Manufacturer's website lists reactivity in human, use in immunohistochemistry in 16 references.

Homer1 (rabbit, Synaptic Systems #160003, 1:1000). Manufacturer's website lists reactivity in human, use in immunohistochemistry in 34 references.

## 10. Eukaryotic cell lines

a. State the source of each eukaryotic cell line used.

566RSC-UBQT cells, a gift from NeuralStem, Inc., were derived from the lower cervical / upper thoracic spinal cord of an 8 week old embryo donated in accordance with NIH and FDA guidelines.

b. Describe the method of cell line authentication used.

These cells are maintained, authenticated, and tested for mycoplasma by NeuralStem, Inc.

c. Report whether the cell lines were tested for mycoplasma contamination.

These cells are maintained, authenticated, and tested for mycoplasma by NeuralStem, Inc.

d. If any of the cell lines used are listed in the database of commonly misidentified cell lines maintained by ICLAC, provide a scientific rationale for their use.

No - 566RSC-UBQT is not in the database, as of version 8.0.

## ► Animals and human research participants

Policy information about [studies involving animals](#); when reporting animal research, follow the [ARRIVE guidelines](#)

### 11. Description of research animals

Provide all relevant details on animals and/or animal-derived materials used in the study.

We studied a total of nine naïve male rhesus macaques (*Macaca mulatta*), aged 6–10 years.

Policy information about [studies involving human research participants](#)

### 12. Description of human research participants

Describe the covariate-relevant population characteristics of the human research participants.

Study did not involve human subjects.